Fusion Engineering and Design 229 (2026) 115788

Contents lists available at ScienceDirect

Fusion Engineering and Design

journal homepage: www.elsevier.com/locate/fusengdes

Multibody dynamics with joint modeling and trajectory optimization for the breeding blanket vertical transporter robot

Hjalte Durocher [a], Christian Bachmann [b], Rocco Mozzillo [c], Günter Janeschitz [d], Xuping Zhang [a,*]

[a] Department of Mechanical and Production Engineering, Aarhus University, Katrinebjergvej 89 G-F, 8200, Aarhus N, Denmark
[b] EUROfusion Consortium, FTD Department, Boltzmannstr. 2, 85748, Garching, Germany
[c] CREATE, Engineering School of Basilicata University, Via dell'Ateneo Lucano 10, 85100, Potenza, Italy
[d] Max–Planck-Institut für Plasmaphysik, Boltzmannstr. 2, 85748, Garching, Germany

ARTICLE INFO

Keywords:
Multibody dynamics
Manipulator
Remote maintenance
Breeding blankets
DEMO

ABSTRACT

The vertical maintenance of breeding blanket (BB) segments weighing as much as 180 t at future fusion power plants like EU-DEMO will be a vital activity enabling plant safety and availability. The BB vertical transporter (BBVT) is a robotic arm with 7 kinematic joints, characterized by a unique and complex mechanical structure, and specifically designed for this challenging task. Sub-centimeter accuracy is required in manipulating the BB segments out of the vacuum vessel through the upper port without collision. Detailed modeling is required before sophisticated control strategies can be developed. In the literature, the dynamic modeling of robotic arms often omits detailed joint modeling to reduce complexity. As such, this work builds on the kinematic model of the BBVT by describing the rigid-body dynamics and filling gaps in the modeling of joints, enabling the loads and motions of actuators and transmission components to be calculated. The previously defined waypoints are interpolated to cubic trajectories and the recursive Newton–Euler inverse dynamics algorithm is applied to obtain the realistic joint loads, helping verify the preliminary design. Then, an inverse-dynamics-based trajectory optimization is performed to estimate the quickest valid BB segment removal times, yielding 41 to 52 min per BB segment or a total of 5.24 days of handling for a 16-sector tokamak. The model and results are also verified with a BBVT simulation in MSC ADAMS. These developments support the further modeling and design of the BBVT to achieve resilient control and safe BB maintenance in a challenging nuclear environment.

1. Introduction

Safe and efficient Breeding blanket (BB) maintenance will be needed for DEMO. Each sector will contain five vertically split BB segments: three on the outboard side weighing up to 180 t each and two on the inboard side weighing up to 125 t each. Due to damage from neutron radiation, these segments must be removed and replaced from time to time. This will be done using a remote handling (RH) tool capable of lifting each BB segment. This is carried to the tokamak complex by a sealed cask which docks via double-doors to the upper port [1]. For removal, the RH tool must grasp the target segment using a standardized conical countersunk hole ("interface") in the exposed upper surface within the upper port using a matching self-locking, folding gripper [2]. Then, the RH tool must lift the BB segment by 120 mm (for outboard segments) or 20 mm (for inboard segments) before tilting the BB segment around the toroidal axis by approximately 5° in order to free the segment from its lower supports [3]. Once the BB segment is lifted and disengaged, it must be maneuvered spatially into the cask through the upper port while avoiding collisions with the vacuum vessel, port walls and neighboring BB segments.

The mechanical design of this RH tool, the BB vertical transporter (BBVT), was introduced in [4] and further developed in [5]. It is a large robotic manipulator which can be analyzed as having 7 serial joints with a PRPRRRR structure (Fig. 1) of prismatic (P) and revolute (R) joints. The kinematic model of the BBVT as a redundant mechanism, analytical procedure for obtaining inverse kinematic solutions, and joint-space waypoints optimized with respect to static loads were presented in [6].

While these previous works have verified the ability of the BBVT to perform the kinematic maneuvers required in the maintenance of DEMO-type BB segments, the joints themselves have not yet undergone

* Corresponding author.
E-mail addresses: hdu@mpe.au.dk (H. Durocher), Christian.Bachmann@euro-fusion.org (C. Bachmann), Rocco.Mozzillo@unibas.it (R. Mozzillo), janeschgu@gmail.com (G. Janeschitz), xuzh@mpe.au.dk (X. Zhang).

https://doi.org/10.1016/j.fusengdes.2026.115788
Received 19 December 2025; Received in revised form 26 March 2026; Accepted 20 April 2026
Available online 4 May 2026

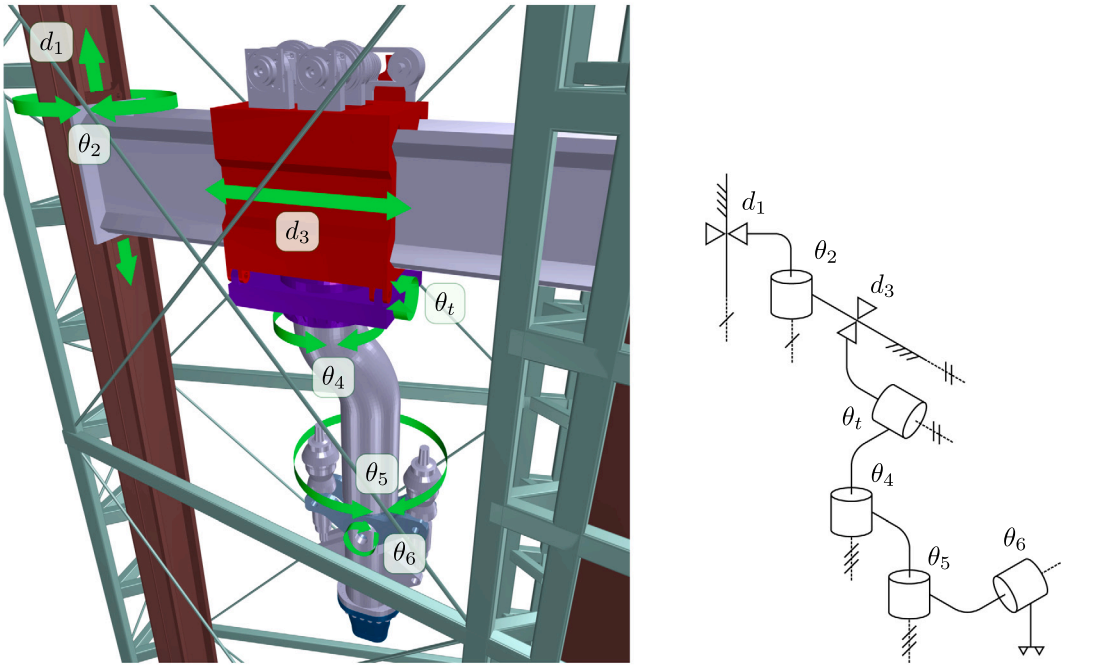

(a) The BBVT inside the cask with its 7 joints labeled. (b) Schematic diagram of the BBVT mechanism.

Fig. 1. Overview of the BBVT robot and its joints (a) in 3-D and (b) in schematic form.

detailed verification with respect to realistic loads expected throughout the task. For this, the kinematic model should be built upon to derive rigid-body dynamic equations of motion, thereby incorporating inertial loads. It is also necessary to elaborate some simplifications embedded in the kinematic model and determine the input–output equations for the joint mechanisms and commercial off-the-shelf (COTS) transmission components such as gearboxes and leadscrews. This will finally allow for the calculation of realistic dynamic actuator loads, verifying the overall joint design in the process.

Thus, this paper presents the BBVT rigid-body dynamics model based on the kinematic model, including the inverse dynamics using the recursive Newton–Euler algorithm, followed by detailed models of the joint mechanisms and COTS components. Then, continuous joint-space trajectories are generated based on the previously developed BB handling waypoints. The inverse dynamics plus joint models are applied to these trajectories to verify the chosen COTS components with respect to the loads. Finally, a straightforward optimization procedure is applied to investigate the minimum realistic handling times for each BB segment. The model is finally verified by simulation of the BBVT optimized trajectory in MSC ADAMS. These developments support the feasibility of the BBVT as an effective remote handling tool for DEMO-type vertical BB segments, and the dynamic model and fully-specified realistic BBVT trajectories can be readily applied and extended in future efforts encompassing modeling, simulation and control development.

In Section 2, the modeling approach for the 7-DoF BBVT is presented, first introducing the rigid-body dynamic model and inverse dynamics solution algorithm, followed by detailed consideration of the joints including parallel and nonlinear mechanisms and COTS components. In Section 3, the inverse dynamics and joint models are applied to validate the BBVT design with respect to the fully specified cubic trajectories for BB segment removal, which are in turn subjected to an optimization procedure which obtains the fastest viable BB segment removal trajectories given the limits of the chosen COTS components. This is followed by a verification of the model by simulation of a BBVT trajectory in ADAMS. Finally, in Section 4, conclusions and future work are laid out.

2. Models

2.1. Rigid-body dynamics

The 7 kinematic joints of the BBVT are illustrated in Fig. 1. The Lagrangian formulation of the BBVT rigid-body dynamics have been derived based on the kinematic model. The preliminary design CAD files are used for obtaining the mass, center of mass, and inertia tensor for each of the 7 robot links and the BB segments, assuming uniform density distributions. With the vector of joint variables $\boldsymbol{\Theta}$ as the minimum set of independent coordinates, the resulting equations of motion can be stated without explicit kinematic constraints as [7]

$$\boldsymbol{M}(\boldsymbol{\Theta})\ddot{\boldsymbol{\Theta}} + \boldsymbol{C}(\boldsymbol{\Theta}, \dot{\boldsymbol{\Theta}}) + \boldsymbol{G}(\boldsymbol{\Theta}) + \boldsymbol{F}_f = \boldsymbol{\tau}, \tag{1}$$

where $\boldsymbol{M}$ is the system mass matrix, $\boldsymbol{C}$ contains centrifugal and Coriolis joint loads, $\boldsymbol{G}$ contains the static joint loads due to gravity, $\boldsymbol{F}_f$ contains dry friction loads, and $\boldsymbol{\tau}$ is the vector of joint torques and forces ("efforts").

Eq. (1) allows the analytical solution to the inverse dynamics problem, i.e. calculating the joint efforts $\boldsymbol{\tau}$ from the robot motion defined by the joint configuration $\boldsymbol{\Theta}$ and its derivatives $\dot{\boldsymbol{\Theta}}$ and $\ddot{\boldsymbol{\Theta}}$. By inputting joint motions which are representative of the robot task, the results can be applied to verify the design of the joints. However, $\boldsymbol{\tau}$ only contains the forces and torques associated the joint variables, i.e., the actuator effort applied by link $i-1$ on link i. As will be detailed in the following subsection, this is not enough information to calculate the heterogeneous loads on the parallel elevator chains and thereby verify the different elevator actuator loads. Therefore, it is more relevant to apply the recursive Newton–Euler algorithm (RNEA) directly in the analysis, as this involves the solution of the full dynamic equilibrium equations for each link.

Another reason to obtain the full link loads using RNEA is to get the normal forces between links, which are needed to calculate the Coulomb friction forces $\boldsymbol{F}_f$. These are based on simple bearing models at each joint.

2.1.1. Summary of the recursive Newton-Euler algorithm

RNEA relies on knowledge of the kinematic model, link mass properties, and the joint positions, velocities and accelerations ($\boldsymbol{\Theta}$, $\dot{\boldsymbol{\Theta}}$ and $\ddot{\boldsymbol{\Theta}}$). The kinematic model for a robot consisting of an open chain of serial links directly provides the relative 3-D position ${}^{i}\boldsymbol{u}_{i+1}$ and orientation matrix ${}^{i}_{i+1}\boldsymbol{R}$ of the rigid-body reference frame of robot link $i+1$ relative to i based on the configuration of the joint connecting the two links. In addition, a velocity transformation matrix ${}^{i+1}_{i}\boldsymbol{T}_{v}$ can be defined:

$$ {}^{i+1}_{i}\boldsymbol{T}_{v} = \begin{bmatrix} {}^{i+1}_{i}\boldsymbol{R} & -{}^{i+1}_{i}\boldsymbol{R}\,{}^{i}\tilde{\boldsymbol{u}}_{i+1} \\ 0 & {}^{i+1}_{i}\boldsymbol{R} \end{bmatrix}, \tag{2} $$

where ${}^{i}\tilde{\boldsymbol{u}}_{i+1}$ is the skew-symmetric matrix formed from ${}^{i}\boldsymbol{u}_{i+1}$. The velocity transformation matrix of Eq. (2) premultiplies the 6-element vector $\boldsymbol{v}_i = \begin{bmatrix} \dot{\boldsymbol{u}}_i^{\top} & \boldsymbol{\omega}_i^{\top} \end{bmatrix}^{\top}$ which collects the 3-D linear and angular velocities of body i, with the result expressing the equivalent motion in the reference frame of body $i+1$ under the assumption that the two frames are instantaneously rigidly connected. The time derivative of Eq. (2) can be found by using the derivative of the rotation matrix $\dot{\boldsymbol{R}} = \tilde{\boldsymbol{\omega}}\boldsymbol{R}$ [8].

The first step of RNEA is to calculate the velocity $\boldsymbol{v}$ and acceleration $\dot{\boldsymbol{v}}$ of each link, starting from the base and going to the outermost link. In considering the motion of joint i, the motion caused by joint i ($\dot{\boldsymbol{\Theta}}_i$ and $\ddot{\boldsymbol{\Theta}}_i$) must be added to the contributions from the motion of link $i-1$, which can be calculated as follows:

$$ \boldsymbol{v}_i = {}^{i}_{i-1}\boldsymbol{T}_{v}\boldsymbol{v}_{i-1} \tag{3} $$

$$ \dot{\boldsymbol{v}}_i = {}^{i}_{i-1}\dot{\boldsymbol{T}}_{v}\boldsymbol{v}_{i-1} + {}^{i}_{i-1}\boldsymbol{T}_{v}\dot{\boldsymbol{v}}_{i-1} \tag{4} $$

Eqs. (3) and (4) are used a second time at each link in order to find the motion at the center of mass $\boldsymbol{v}_{c_i}$ and $\dot{\boldsymbol{v}}_{c_i}$. The inertia forces and moments are then calculated using Newton's and Euler's equations, respectively:

$$ \boldsymbol{F}_{c_i} = m_i\ddot{\boldsymbol{u}}_{c_i} \tag{5} $$

$$ \boldsymbol{N}_{c_i} = (\boldsymbol{I}\dot{\boldsymbol{\omega}} + \tilde{\boldsymbol{\omega}}\boldsymbol{I}\boldsymbol{\omega})_{c_i}\,. \tag{6} $$

The 6-element vector collecting the inertial forces and moments $\boldsymbol{\mathcal{F}}_{c_i} = \begin{bmatrix} \boldsymbol{F}_{c_i}^{\top} & \boldsymbol{N}_{c_i}^{\top} \end{bmatrix}^{\top}$ is then transformed back to each link frame using force transformations, which are equivalent to the transposes of the previously used velocity transformations:

$$ {}^{i}_{i+1}\boldsymbol{T}_{f} = {}^{i+1}_{i}\boldsymbol{T}_{v}^{\top}. \tag{7} $$

Finally, the full reaction forces required to balance the inertial forces on link i plus the forces applied by link $i+1$ are solved, working from the outermost link to the base:

$$ \boldsymbol{\mathcal{F}}_i = {}^{i}_{c_i}\boldsymbol{T}_{f}\boldsymbol{\mathcal{F}}_{c_i} + {}^{i}_{i+1}\boldsymbol{T}_{f}\boldsymbol{\mathcal{F}}_{i+1}. \tag{8} $$

2.2. Joint models

Although the dynamic model can be used to calculate the joint efforts associated with a particular configuration and motion of the BBVT, many details about the joints themselves must be fleshed out in order to calculate the actuator loads. This entails modeling the proposed joint transmission components as summarized in Fig. 2, including some mechanisms with nonlinear input–output equations. Also, although the kinematic model makes the simplification of representing the three parallel rigid chains of the elevator as a unified prismatic joint (d_1), we are interested in obtaining the load in each chain separately while maintaining the assumption of synchronized motion.

2.2.1. Nonlinear joints

Joints 2, t, and 6 are implemented as nonlinear mechanisms with effective transmission ratios which vary according to the joint position. This in turn affects the total inertias of these joints. The kinematics of joint t, the trolley tilting mechanism, have been described in detail in [9]. The remaining two mechanisms have in common that they convert the linear input motion produced by a leadscrew into rotational output motion. With reference to the schematic diagrams in Figs. 3 and 4(b), the configuration-dependent transmission ratios for joints 2 and 6 are given by:

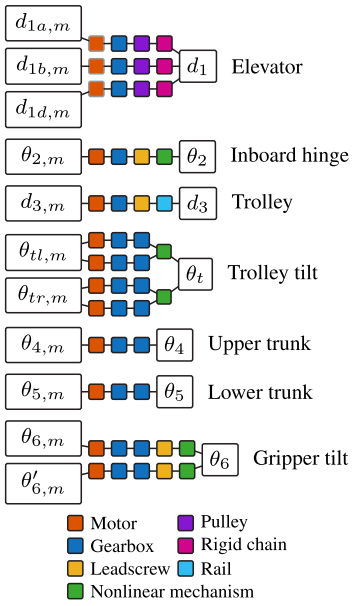

Fig. 2. The structure of each joint from actuator(s) (left) to output (right).

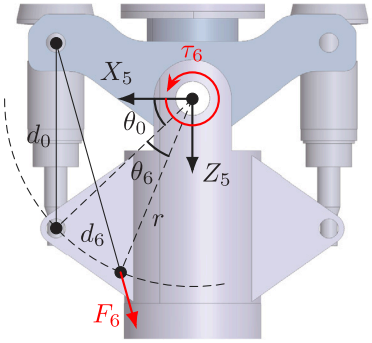

Fig. 3. Schematic diagram of the joint 6 mechanism.

$$ d_2 = -h\tan\theta_2 \tag{9} $$

$$ \frac{\dot{d}_2}{\dot{\theta}_2} = -\frac{h}{\cos^2\theta_2} \tag{10} $$

$$ d_6 = \sqrt{2r^2\left(1-\cos\theta_6\right) + 2rd_0\left(\sin\left(\theta_0+\theta_6\right) - \sin\theta_0\right) + d_0^2} \tag{11} $$

$$ \frac{\dot{d}_6}{\dot{\theta}_6} = \frac{r^2\sin\theta_6 + rd_0\cos\left(\theta_0+\theta_6\right)}{\sqrt{2r^2\left(1-\cos\theta_6\right) + 2rd_0\left(\sin\left(\theta_0+\theta_6\right) - \sin\theta_0\right) + d_0^2}} \tag{12} $$

The symbols in Eqs. (9)–(12) are specific to the context of each mechanism as labeled in the respective schematic diagrams. The constants are: $h = 5.55$, $r = 0.8277$, $P_0 = [0.6, 0.57017962]$, $d_0 = 0.8151$ and $\theta_0 = \mathrm{atan2}\left(P_{0,y}, P_{0,x}\right)$.

Eqs. (10) and (12) specify the configuration-dependent transmission ratios of the two joints in terms of the ratio of input and output velocities. Knowledge of the transmission ratios also allows the calculation of input and output torques/forces. A complication arises for joint 6 due to the use of a mirror mechanism, where the $\theta'_6 = -\theta_6$ but $d'_6 \neq -d_6$. For the analysis it is assumed that the output joint load is shared equally between the two leadscrews, resulting in differing actuator loads on each side due to the asymmetric nature of the joint.

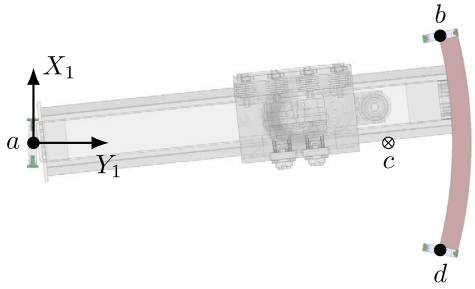

(a) The elevator with center of mass c and vertical rigid chain supports at a, b and d.

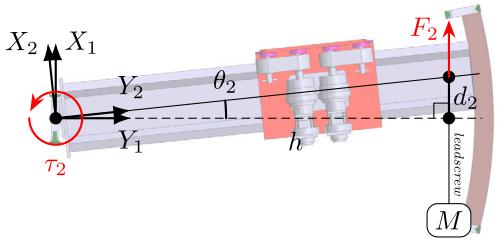

(b) The inboard hinge (joint 2) mechanism.

Fig. 4. Top-down view of the BBVT.

2.2.2. Elevator rigid chains

It is assumed that the three elevator chains move in sync as one prismatic joint, attached to a single disjoint rigid body link consisting of the three skids and the toroidal rail (but not the radial rail), as illustrated in Fig. 4(a). At the same time, the unique load on each elevator chain and actuator is of interest. The dynamic balance of forces and moments for the elevator link with inboard support at a coincident with the origin of the elevator link frame $\{1\}$, outboard supports at b and d, center of mass at c, and applied loads from the trolley at link frame $\{2\}$ can be written as:

$$\Sigma \boldsymbol{F} = \boldsymbol{F}_c = \boldsymbol{F}_a + \boldsymbol{F}_b + \boldsymbol{F}_d - \boldsymbol{F}_2 \tag{13}$$

$$\begin{aligned}\Sigma \boldsymbol{M} = \boldsymbol{P}_c \times \boldsymbol{F}_c =& \boldsymbol{P}_b \times \boldsymbol{F}_b + \boldsymbol{M}_b + \boldsymbol{P}_d \times \boldsymbol{F}_d \\ &+ \boldsymbol{M}_d - \boldsymbol{P}_2 \times \boldsymbol{F}_2 - \boldsymbol{M}_2 + \boldsymbol{M}_a,\end{aligned} \tag{14}$$

where P are spatial position vectors, F are 3-element force vectors, and M are 3-element moment vectors. With reference to Fig. 4(a), the vector subscripts indicate whether they are associated with chain a, b or d, or the elevator center of mass c, or the trolley 2. The full loads on the trolley F_2 and M_2 can be obtained using RNEA. All position vectors are expressed relative to the elevator link frame $\{1\}$ and all forces and moments are aligned with this frame as well (so rotation matrices are not explicitly written). The system of equations can be solved when the support conditions are considered. Namely, no moments are reacted directly at any support except for the radial moment $\boldsymbol{M}_{a,y}$ at the inboard support, and the outboard skids only support vertical reactions while the inboard skids support reactions in all directions. Eqs. 13 can then be solved to find the six unknown reactions. The results are given by Eq. (B.1) to (B.6) in Appendix B. Specifically, the reactions of interest representing the vertical chain loads are $F_{a,z}$, $F_{b,z}$ and $F_{d,z}$.

2.2.3. Off-the-shelf components

A variety of COTS components have been identified for the preliminary design of the BBVT joints. Other than the elevator (for which no specific actuator has yet been specified), all joints employ MOOG MD Series JSC3-075 electric motors. The gearboxes and power screws chosen for each joint are summarized in Table A.1. The transmission ratio/pitch and inertia of each component is recorded from the manufacturer datasheets. In addition, limits for dynamic load, velocity and power are recorded, as they are necessary for the trajectory optimization in the sequel.

2.2.4. Actuator loads

Inspecting Fig. 2, it is evident that while there are 7 variables which together define the joint configuration vector Θ, the use of parallel actuators in joints 1, t and 6 means that the number of unique actuator loads of interest is more than 7. For joint t, the layout is such that loads are equally distributed between the two actuators, while the differential loads on the joint 1 and 6 actuators have been addressed in the previous subsections. The loads of interest can be summarized as

$$\boldsymbol{\tau}' = \begin{bmatrix}\tau_{1,a} & \tau_{1,b} & \tau_{1,d} & \tau_2 & \tau_3 & \tau_t & \tau_4 & \tau_5 & \tau_6 & \tau_6'\end{bmatrix}^\top, \tag{15}$$

where $\tau_{1,a}$, $\tau_{1,b}$ and $\tau_{1,d}$ represent the actuators of the three rigid chains and τ_6' is the mirror actuator of the gripper tilting joint (θ_6). Analogously, the set of matching joint motions can be defined:

$$\boldsymbol{\Theta}' = \begin{bmatrix}\theta_1 & \theta_1 & \theta_1 & \theta_2 & \theta_3 & \theta_t & \theta_4 & \theta_5 & \theta_6 & \theta_6'\end{bmatrix}^\top. \tag{16}$$

The total inertia of the jth actuator's transmission related to the joint output is calculated as

$$B_j = \sum_{k}^{n_s-1} b_{j,k}\eta_{j,k+1}^2 \frac{1}{n_{j,k}} \quad \text{for} j = 1, 2, \ldots, 10, \tag{17}$$

where n_s is the number of transmission stages in the joint to which actuator j belongs, $b_{j,k}$ is the inertia of the joint component at stage k related to its own output, $\eta_{j,k+1}$ is the transmission ratio of the component at stage $k+1$, and $n_{j,k}$ is the number of branches between the actuator and stage k. It should be noted that the position-dependent transmission ratios of the joints with nonlinear mechanisms (2, t and 6) result in time-varying inertias for these joints.

Finally, the actuator loads can be found:

$$\boldsymbol{\tau}_m = \boldsymbol{\eta}_{inv}(\boldsymbol{\Theta})\left(\boldsymbol{B}(\boldsymbol{\Theta})\ddot{\boldsymbol{\Theta}}' + \boldsymbol{\tau}'(\boldsymbol{\Theta}, \dot{\boldsymbol{\Theta}}, \ddot{\boldsymbol{\Theta}})\right), \tag{18}$$

where $\boldsymbol{B}$ and $\boldsymbol{\eta}_{inv}$ are diagonal matrices containing the position-dependent total joint inertias and inverse transmission ratios, respectively.

3. Generation and optimization of BB handling trajectories

3.1. Optimization algorithm

The waypoints proposed in the previous kinematic study can be used as a starting point for generating complete joint-space trajectories in the form of differentiable polynomials defining the time evolution of the joint positions. Solving for the polynomial coefficients requires specifying the duration of each trajectory part and the desired derivatives of the position at each waypoint. RNEA and the joint models previously described can then be applied to calculate the required dynamic loads and motions of the actuators and the other joint components throughout the trajectory. The results can be compared where available against the manufacturer limits on load, velocity and power, including safety factors. Not only does this procedure allow for verification of the BBVT joint design with respect to a given trajectory, but also provides a way to estimate the fastest viable trajectory for a given design via optimization.

The algorithm for minimizing the duration of a BB segment handling trajectory based on the procedure just described is summarized in Fig. 5. The optimization criteria are the component "limit ratios," i.e., the ratio of each value of interest (static load, dynamic load, velocity, power) to the corresponding component limit while taking safety factors into account for loads. Specifically, the maximum limit ratio (MLR) for any component across 100 samples is identified per trajectory part. In the subsequent iteration, the duration of the trajectory part is multiplied by this MLR to obtain the new duration. For a viable

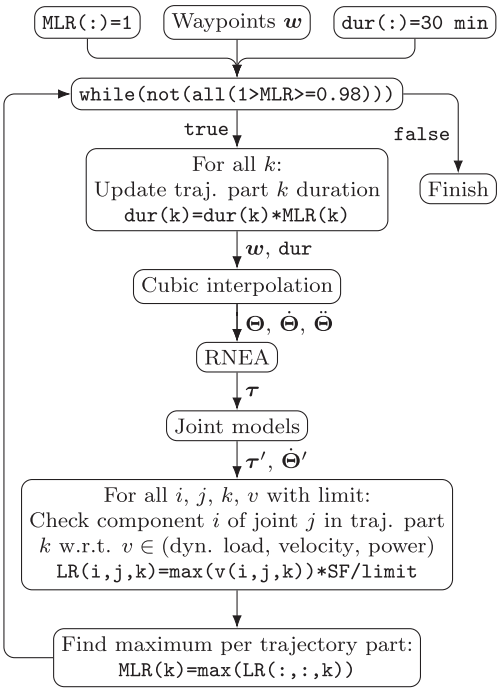

Fig. 5. Flowchart of the trajectory optimization algorithm, which is repeated for each of the 5 BB segment shapes.

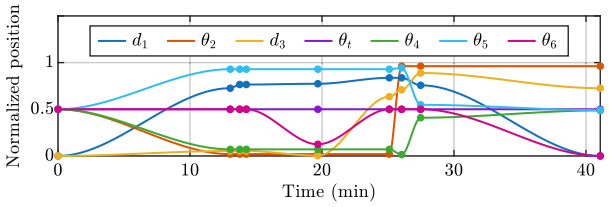

Fig. 6. Inboard right BB segment removal trajectory in normalized joint-space. Dots represent the joint-space waypoints.

trajectory, it is clear that all MLRs must be less than 1.0. On the other hand, the fastest viable trajectory should have MLRs close to 1.0 for all trajectory parts.

A few details should be noted regarding the optimization algorithm. First, due to the polynomial continuity conditions, changing the duration of one trajectory part also affects the neighboring trajectory parts. For this reason, it is crucial for convergence that the durations of all trajectory parts are adjusted simultaneously in each iteration. Second, the choice to use cubic splines (continuous piecewise polynomials) for interpolating the waypoints, though common practice for industrial robots, is relatively arbitrary. They result in faster trajectories than higher-order polynomials such as quintics or septics, but are not continuous in terms of jerk. Third, boundary conditions are imposed such that the BBVT comes to a full stop at each waypoint to avoid overshoot which could otherwise result in collisions. Finally, it should be noted that static and dynamic load limits are handled differently. If a static load limit is violated, the optimization cannot proceed since changing the BBVT speed will have no effect.

3.2. Results

Fig. 6 shows a joint-space trajectory for removal of the inboard right BB segment after optimization, given the current BBVT design. The durations of the optimized trajectories for each BB segment are

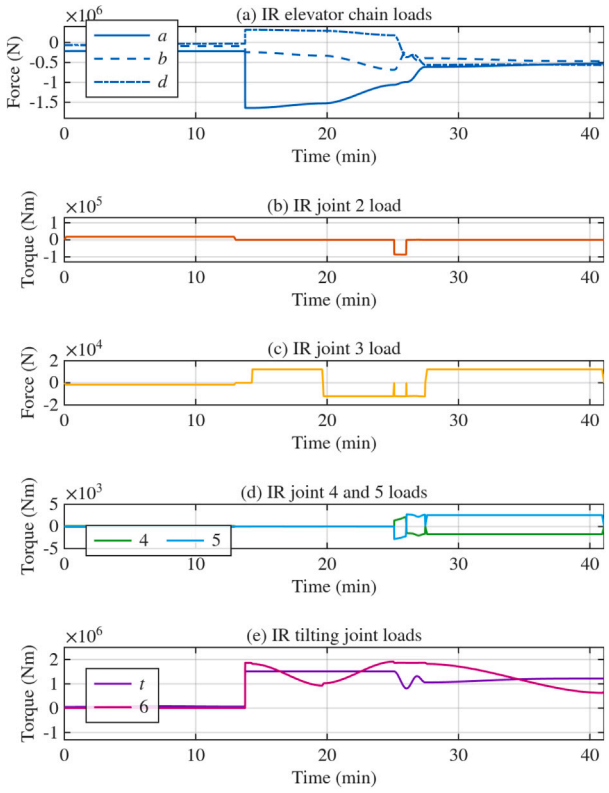

Fig. 7. Joint loads throughout the inboard right (IR) BB segment removal trajectory. The BB segment is picked up at 13 min 45 s.

50 min, 52 min, 52 min, 41 min and 41 min for the outboard middle, outboard left, outboard right, inboard right and inboard left BB segments, respectively. These represent the first realistic estimates of the handling times required for the maintenance of DEMO BB segments based on detailed dynamic modeling of the BBVT. It should be noted, however, that the trajectories do not take into account extra time for BB segment grasping and preloading. Still, the results suggest that a realistic if somewhat optimistic estimate of the total BB handling time required for maintenance of the BB segments in all 16 DEMO sectors is about 5.24 days.

Fig. 7 shows the joint loads (not actuator loads) associated with the trajectory in Fig. 6. It is evident that the loads on joints 2, 3, 4 and 5 are dominated by dry friction rather than dynamic or static loads. Looking at the elevator chains, it is notable that chain d (the outboard left chain) experiences compression forces in the period after picking up the BB segment. Indeed, the results predict that the opposing outboard chain experiences compression forces when picking up each of the lateral BB segments, whether inboard or outboard. This highlights the need for a "rigid" chain solution, as has been explored in the BBVT concept design. Both of the tilting joints experience very high moment loads as expected due to the off-center lifting. Elevator and tilting joint loads for the other four BB segments' removal trajectories are given in Fig. C.9.

3.3. Verification

As an extra verification of the model and results, a simulation was run using the commercial multibody simulation software MSC ADAMS. The predicted joint torques corresponding to the inboard right BB segment removal trajectory after picking up the BB segment were input to the model, with accurate starting configuration as shown in Fig. 8(a). Given the relatively long simulation time, 10 million simulation time

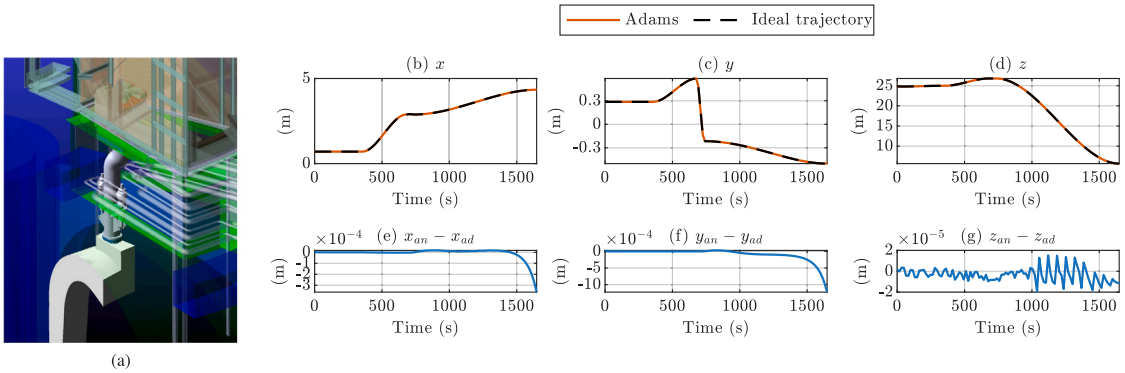

Fig. 8. Simulation of the inboard right BB segment handling in ADAMS using the predicted joint torques τ as input. The simulation is started from when the BB is grasped as shown in (a). The resulting motion of the gripper in the simulation is compared to the ideal trajectory in (b)–(d), while (e)–(g) show just the errors.

steps were used to obtain good results with minimal numerical errors. Indeed, the results shown in Fig. 8 indicate good agreement between the Cartesian path traveled by the tip of the BBVT gripper in the simulation and the ideal trajectory. The overall RMSE is 1.1953×10^{-4} m.

4. Conclusion

The BBVT will serve a critical role in ensuring the safety and availability of DEMO through effective BB segment handling. This task will require sub-centimeter accuracy to remove and insert each of the BB segments from the tightly constrained vacuum vessel and upper port without collision in a nuclear environment which is also likely to be hot and unilluminated. Achieving this task requires detailed modeling of the BBVT as a massive 7-DoF robotic manipulator in order to build towards the design of resilient and reliable control strategies.

This work has built on previous modeling of the BBVT in which in collision-free BB handling waypoints and a practical kinematic model were presented. The extension of the kinematic model into rigid-body dynamics has been described, and the previous gaps in nonlinear joint modeling have been filled, enabling the loads and motions of the 10 actuators of interest and other joint components to be investigated in detail. The joint-space waypoints were interpolated with cubic splines, resulting in fully-specified trajectories. By applying the RNE algorithm for inverse dynamics to the trajectories, the realistic joint loads were obtained, against which the preliminary joint designs were verified in the sense that the manufacturer limits for COTS components were not exceeded. The joint models, knowledge of component limits, trajectory generation function, and inverse dynamics algorithm were then synthesized to implement an optimization procedure by which the fastest viable cubic trajectories for BB segment removal using the preliminary BBVT design were obtained. The results indicate that the outboard and inboard lateral segments require 52 min and 41 min of handling time, respectively, starting from when the BBVT starts moving out of the cask to when the target BB segment is held still in the cask and excluding extra time for grasping and preloading. This leads to a realistic but likely optimistic estimate of 5.24 days total of BB handling time for removing and inserting all the BB segments of the DEMO tokamak with 16 sectors. Finally, the veracity of the model and results were verified using a rigid-body dynamic simulation in MSC ADAMS.

This work has focused on the preliminary BBVT joint-space trajectories for BB manipulation, whereas two critical aspects of the BB handling task have not been considered, namely grasping and preloading. These will require further specialization of the model due to the prevalence of different effects such as contact forces and flexible deformations. Indeed, major sources of joint and link elasticity throughout whole BB task must be modeled in the future, as deflections and vibrations must be counteracted by any effective control solutions.

CRediT authorship contribution statement

Hjalte Durocher: Writing – original draft, Visualization, Validation, Software, Resources, Methodology, Investigation, Formal analysis, Data curation, Conceptualization. **Christian Bachmann:** Funding acquisition, Conceptualization. **Rocco Mozzillo:** Conceptualization. **Günter Janeschitz:** Conceptualization. **Xuping Zhang:** Writing – review & editing, Supervision, Project administration, Funding acquisition.

Declaration of competing interest

The authors declare the following financial interests/personal relationships which may be considered as potential competing interests: Xuping Zhang reports financial support was provided by European Consortium for the Development of Fusion Energy. Hjalte Durocher reports financial support was provided by European Consortium for the Development of Fusion Energy. If there are other authors, they declare that they have no known competing financial interests or personal relationships that could have appeared to influence the work reported in this paper.

Acknowledgments

This work has been carried out within the framework of the EUROfusion Consortium, funded by the European Union via the Euratom Research and Training Programme (Grant Agreement No 101052200 – EUROfusion). Views and opinions expressed are however those of the author(s) only and do not necessarily reflect those of the European Union or the European Commission. Neither the European Union nor the European Commission can be held responsible for them.

Appendix A. COTS joint components

See Table A.1.

Appendix B. Elevator chain dynamic reaction loads

The following equations give the six unknown dynamic reactions at the inboard ($\{a\}$) and outboard right and left ($\{b\}$, $\{d\}$) skids assuming the skids and toroidal beam constitute a single rigid body experiencing inertial forces at the shared center of mass $\{c\}$ and transferred loads from the distal robot links through the trolley at $\{2\}$ based on the recursive Newton–Euler algorithm. The vertical reactions ($_z$) are assumed taken by the rigid chains, while the rest are reacted by the skid rails. The unspecified reactions are assumed to be zero based on the support conditions (see the equations in Box I).

Table A.1
Off-the-shelf joint transmission components.

Joint	Outer gearbox	Inner gearbox	Leadscrew
1	Brevini SC18004 (559.2)	–	–
2	Wittenstein TK+ 110 MF (20)	–	Ewellix PRU 60x20
3	Wittenstein TK+ 110 MF (20)	–	Ewellix PRU 60x20
t	Sumitomo Fine Cyclo A-series FC Type A25 (119)	Wittenstein TP+ 4000 MA (154)	–
4	Sumitomo Fine Cyclo A-series FC Type A25 (89)	Wittenstein TP+ 2000 MA (22)	–
5	Sumitomo Fine Cyclo A-series FC Type A25 (89)	Wittenstein TP+ 2000 MA (22)	–
6	Sumitomo Fine Cyclo A-series FC Type A35 (89)	Wittenstein TP+ 2000 MA (30.25)	Ewellix HRC 99x20

$$F_{a,x} = F_{2,x} + F_{c,x} \tag{B.1}$$

$$F_{a,y} = F_{2,y} + F_{c,y} \tag{B.2}$$

$$F_{a,z} = \begin{aligned} &\frac{-1}{P_{b,x}P_{d,y} - P_{b,y}P_{d,x}} \left(M_{2,x}P_{b,x} + M_{2,y}P_{b,y} - M_{2,x}P_{d,x} - M_{2,y}P_{d,y} + M_{c,x}P_{b,x} + M_{c,y}P_{b,y} - M_{c,x}P_{d,x} - M_{c,y}P_{d,y} \right. \\ &-F_{2,z}P_{b,x}P_{d,y} + F_{2,z}P_{b,y}P_{d,x} + F_{c,x}P_{b,y}P_{c,z} - F_{c,y}P_{b,x}P_{c,z} + F_{c,z}P_{b,x}P_{c,y} - F_{c,z}P_{b,y}P_{c,x} \\ &\left. - F_{c,z}P_{b,x}P_{d,y} + F_{c,z}P_{b,y}P_{d,x} - F_{c,x}P_{c,z}P_{d,y} + F_{c,y}P_{c,z}P_{d,x} + F_{c,z}P_{c,x}P_{d,y} - F_{c,z}P_{c,y}P_{d,x} \right) \end{aligned} \tag{B.3}$$

$$F_{b,z} = -\frac{M_{2,x}P_{d,x} + M_{2,y}P_{d,y} + M_{c,x}P_{d,x} + M_{c,y}P_{d,y} + F_{c,x}P_{c,z}P_{d,y} - F_{c,y}P_{c,z}P_{d,x} - F_{c,z}P_{c,x}P_{d,y} + F_{c,z}P_{c,y}P_{d,x}}{P_{b,x}P_{d,y} - P_{b,y}P_{d,x}} \tag{B.4}$$

$$F_{d,z} = \frac{M_{2,x}P_{b,x} + M_{2,y}P_{b,y} + M_{c,x}P_{b,x} + M_{c,y}P_{b,y} + F_{c,x}P_{b,y}P_{c,z} - F_{c,y}P_{b,x}P_{c,z} + F_{c,z}P_{b,x}P_{c,y} - F_{c,z}P_{b,y}P_{c,x}}{P_{b,x}P_{d,y} - P_{b,y}P_{d,x}} \tag{B.5}$$

$$M_{a,z} = M_{2,z} + M_{c,z} - F_{c,x}P_{c,y} + F_{c,y}P_{c,x} \tag{B.6}$$

Box I.

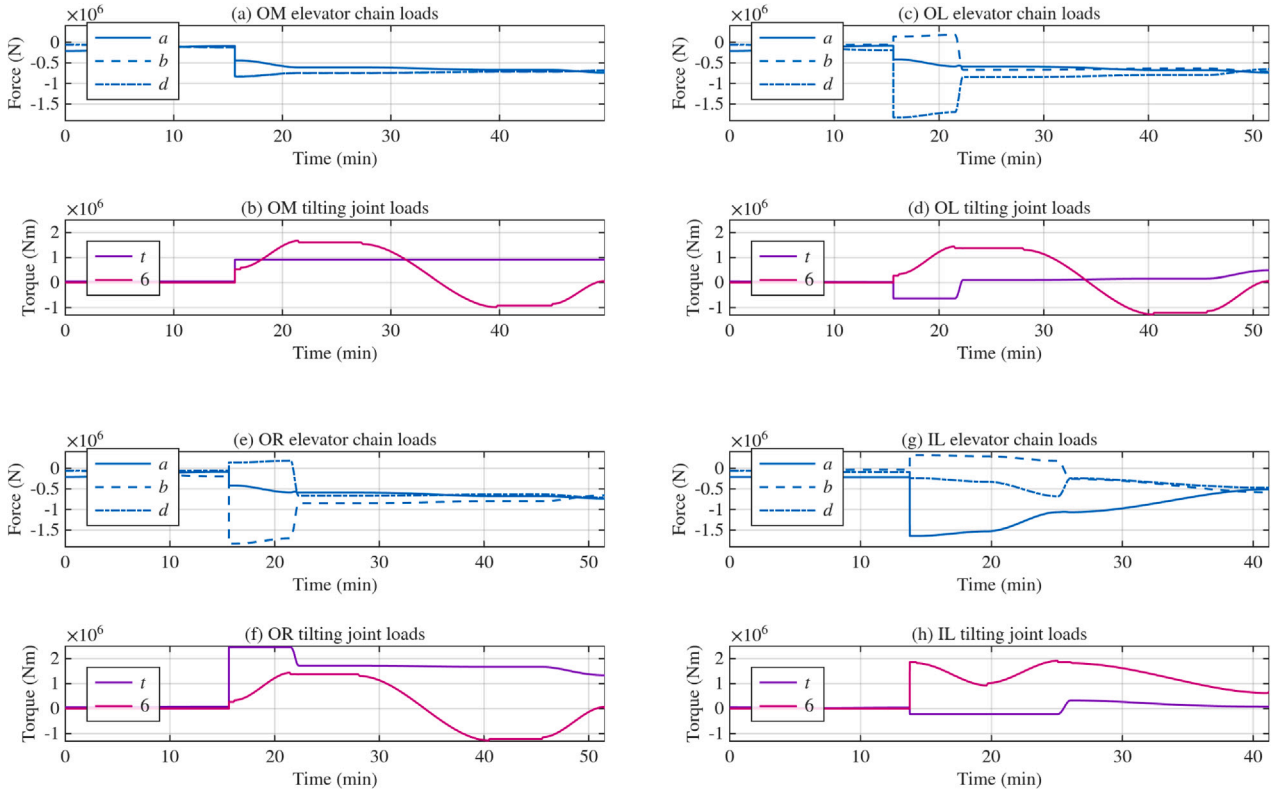

Fig. C.9. Loads on the BBVT elevator and tilting joints throughout the BB segment removal trajectories. (a)–(b): Outboard middle segment, (c)–(d): Outboard left segment, (e)–(f) Outboard right segment, (g)–(h) Inboard left segment.

Appendix C. Additional joint loads

See Fig. C.9.

Data availability

No data was used for the research described in the article.

References

[1] M. Coleman, N. Sykes, D. Cooper, D. Iglesias, R. Bastow, A. Loving, J. Harman, Concept for a vertical maintenance remote handling system for multi module blanket segments in DEMO, Fusion Eng. Des. 89 (9) (2014) 2347–2351, http://dx.doi.org/10.1016/j.fusengdes.2014.02.047.

[2] T. Steinbacher, C. Bachmann, C. Gliss, G. Janeschitz, R. Mozzillo, Design of the gripper interlock that engages with the DEMO breeding blanket during remote maintenance, Fusion Eng. Des. 193 (2023) 113641, http://dx.doi.org/10.1016/j.fusengdes.2023.113641.

[3] C. Bachmann, C. Gliss, T. Härtl, F. Hernandez, I. Maione, T. Steinbacher, Z. Vizvary, Mechanical support concept of the DEMO breeding blanket, Fusion Eng. Des. 173 (2021) 112840, http://dx.doi.org/10.1016/j.fusengdes.2021.112840.

[4] C. Bachmann, C. Gliss, G. Janeschitz, T. Steinbacher, R. Mozzillo, Conceptual study of the remote maintenance of the DEMO breeding blanket, Fusion Eng. Des. 177 (2022) 113077, http://dx.doi.org/10.1016/j.fusengdes.2022.113077.

[5] C. Bachmann, G. Janeschitz, P. Fanelli, C. Gliss, P. Mollicone, M. Muscat, C. Stefanini, T. Steinbacher, J.V. Domínguez, F. Vigano, F. Vitolo, R. Mozzillo, Progress in the development of the in-vessel transporter and the upper port cask for the remote replacement of the DEMO breeding blanket, Fusion Eng. Des. 194 (2023) 113715, http://dx.doi.org/10.1016/j.fusengdes.2023.113715.

[6] H. Durocher, C. Bachmann, R. Mozzillo, G. Janeschitz, X. Zhang, Inverse Kinematics and Statics-Based Motion Planning of a 7-DoF Transporter for DEMO-Type Breeding Blankets, Machines (2026) http://dx.doi.org/10.3390/machines14050469.

[7] J.J. Craig, Introduction to Robotics: Mechanics and Control, third ed.

[8] A.A. Shabana, Computational Dynamics, first ed., John Wiley & Sons, Ltd, 2010, http://dx.doi.org/10.1002/9780470686850.

[9] H. Durocher, C. Bachmann, R. Mozzillo, G. Janeschitz, X. Zhang, A Spatial Five-Bar Linkage as a Tilting Joint of the Breeding Blanket Transporter for the Remote Maintenance of EU DEMO, Machines 13 (5) (2025) 371, http://dx.doi.org/10.3390/machines13050371.